Periodic Motion of Large DNA Molecules during Steady Field Gel Electrophoresis

Hidehiro Oana, Yuichi Masubuchi, Mitsuhiro Matsumoto, Masao Doi,* Yukiko Matsuzawa,† and Kenichi Yoshikawa†

School of Engineering and Graduate School of Human Informatics, Nagoya University, Nagoya 464-01, Japan

Received April 26, 1994; Revised Manuscript Received July 14, 1994®

ABSTRACT: Direct observation of individual T4 DNA molecules during steady field gel electrophoresis was carried out with fluorescence microscopy. Statistical analyses of the image data show that (i) DNA molecules change their conformation and velocity periodically even under a steady field, (ii) the characteristic time of the periodic motion decreases with an increase of the electric field and with a decrease of the gel concentration, and (iii) the rear end of DNA shows a periodic stick–slip motion, while the front end moves with almost constant speed. A possible interpretation for the periodic behavior is presented.

1. Introduction

Gel electrophoresis is a technique widely used to separate DNA fragments of different lengths. Despite its wide usage, the detail of the underlying physics is not fully understood. The migration velocity of a DNA is a nonlinear function of the applied field, and its theoretical prediction has not been successful, especially when the applied field is time dependent.[1,2]

A large number of studies have been made to understand the nonlinear transport phenomena in the gel electrophoresis. A powerful technique is fluorescence microscopy,[3] which enables a direct observation of the motion of DNA molecules during gel electrophoresis. By this technique, it has been found that even in the steady field, the dynamics of the DNA molecules is rather complex.[4–9] As a DNA migrates through a gel network, it repeats a cycle of elongation and contraction. The DNA is elongated when it is hooked by an obstacle, while it contracts when it slides off the obstacle. This behavior has been described as a cyclic or inch-worm motion.

Similar behavior of DNA has also been found by computer simulations.[10–14] Deutsch et al.[10] solved a Langevin equation for a DNA chain in a field of obstacles and found that the velocity and the radius of gyration of DNA fluctuate violently around the mean value. Essentially the same phenomena have also been observed for other models.[11–14] Furthermore, it has been conjectured that the cyclic motion is related to the phenomena of the minimum in the mobility in the field inversion gel electrophoresis (FIGE).[15]

While the dynamics of DNA has been studied extensively by computer simulations, there have been few quantitative studies on the actual conformational change of DNA molecules. We have conducted a statistical analysis of the video images of DNA molecules obtained by fluorescence microscopy and reported preliminary results.[9] In this paper, we describe the results in more detail and also give their gel concentration dependence.

2. Experimental Section

2.1. Materials. Bacteriophage T4 DNA (166kbp; contour length, 55 μm) was purchased from Nippon Gene. Agarose (FMC SeaKem LE) was dissolved in distilled water, using a microwave oven. After the agarose solution was cooled to about 60 °C, Tris-borate (TBE; pH7.8) buffer, T4 DNA, ethidium bromide (EB; intercalating fluorescent dye), and 2-mercaptoethanol (2-ME; as an antioxidant) were added to the solution. The final concentrations are as follows: T4 DNA, 0.15 μM (in nucleotide); EB, 0.15 μM; Tris-borate, 45 mM; EDTA, 1.25 mM; 2-ME, 4% (v/v); agarose, 0.75% (w/v), 0.9% (w/v), 1.25% (w/v), or 1.5% (w/v). Under these conditions, the intercalated EB has a negligible effect on the static properties of DNA.[16,17]

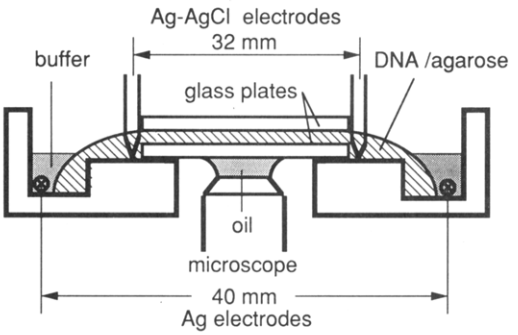

Figure 1. Schematic cross-sectional view of the gel electrophoresis cell specially designed for direct observation. The buffer wells, each with an Ag electrode, are filled with ×0.5 TBE buffer.

2.2. Gel Electrophoresis and Direct Observation. The observation of DNA molecules during gel electrophoresis was carried out in a specially-designed gel electrophoresis cell shown in Figure 1. The cell was prepared as follows. A DNA/agarose solution was placed on a 30 mm × 40 mm glass plate and covered by another glass plate of the same size, and then the whole solution was cooled to be a gel. The thickness of the agarose layer was about 100 μm, which is sufficient to eliminate boundary effects of the glass plates.[16] The electric field was applied by a potentiostat through a pair of silver wire electrodes 40 mm apart. To compensate the polarization effect of the Ag electrodes, the cell had another pair of electrodes (Ag–AgCl) 32 mm apart. The Ag–AgCl electrodes monitor the actual field strength in the observation area, and the applied field strength was adjusted to keep the monitored field constant. The gel was excited by 520 nm UV, and individual DNA molecules were observed as fluorescence images with an inverted microscope (Nikon TMD) equipped with a ×100 oil-immersed objective lens. The images were recorded on S-VHS video tapes with a high sensitivity SIT camera and an image processor, Argus10 (Hamamatsu Photonics).

Two series of experiments were done. First, the gel concentration C_{gel} was fixed at 0.9 wt % and the strength of the electric field E was changed as 2, 4, 6, and 8 V/cm. Second, E was fixed at 8 V/cm and C_{gel} was varied as 0.75, 0.9, 1.25, and 1.5 wt %. All experiments were done at room temperature (about 20 ± 1 °C).

2.3. Image Analyses. The recorded images were processed by a programmable image analysis system PIAS3 (PIAS) which

* To whom correspondence should be addressed.
† Graduate School of Human Informatics.
® Abstract published in *Advance ACS Abstracts,* September 1, 1994.

0024-9297/94/2227-6061$04.50/0

converts the analog image data into digital data of 512 × 512 pixels with 256 degrees of brightness.

After elimination of the background noise with filters of PIAS3, the DNA image function $I(x,y,t)$, which takes 1 if the pixel (x, y) is brighter than a certain threshold or 0 if it is not, is obtained as a function of t. Here the x-axis is taken along the direction of the applied field. Then, the position vector of the center of mass of a DNA molecule $\mathbf{r}(t) = (r_x(t), r_y(t))$ was calculated by

$$r_x(t) = \sum_x \sum_y xI(x,y,t)/I_0 \tag{1}$$

$$r_y(t) = \sum_x \sum_y yI(x,y,t)/I_0 \tag{2}$$

where

$$I_0 = \sum_x \sum_y I(x,y,t) \tag{3}$$

From the series of data $\mathbf{r}(t)$, the center of mass velocity $v_x(t)$ along the applied field was computed by

$$v_x(t) \equiv \frac{r_x\left(t + \frac{1}{2}\Delta t\right) - r_x\left(t - \frac{1}{2}\Delta t\right)}{\Delta t} \tag{4}$$

Although the video image was obtained every $^1/_{30}$ s, Δt was taken to be 0.4 s, since small Δt gives large statistical fluctuations of $v_x(t)$.

To characterize the size of a DNA molecule, the radii R_l and R_s ($R_l > R_s$) which are along the two principal axes repsectively were computed as

$$R_l(t) = \left[\frac{1}{2}(M_{xx} + M_{yy}) + \frac{1}{2}[(M_{xx} - M_{yy})^2 + 4M_{xy}{}^2]^{1/2}\right]^{1/2} \tag{5}$$

$$R_s(t) = \left[\frac{1}{2}(M_{xx} + M_{yy}) - \frac{1}{2}[(M_{xx} - M_{yy})^2 + 4M_{xy}{}^2]^{1/2}\right]^{1/2} \tag{6}$$

where M_{xx}, M_{yy}, and M_{xy} are the components of the two-dimensional radius of gyration tensor defined as

$$M_{xx} = \sum_x \sum_y (x - r_x)^2 I(x,y,t)/I_0 \tag{7}$$

$$M_{yy} = \sum_x \sum_y (y - r_y)^2 I(x,y,t)/I_0 \tag{8}$$

$$M_{xy} = \sum_x \sum_y (x - r_x)(y - r_y) I(x,y,t)/I_0 \tag{9}$$

We use R_l and R_s separately here instead of $R_g = [\frac{3}{2}(R_l^2 + R_s^2)]^{1/2}$ as in ref 9 to characterize the size of DNA, because thus defined R_g overestimates the radius of gyration when the DNA is extremely elongated in one direction.

Tracing the image of each DNA molecule was possible for about 25 s at most in the usual measurement, due to the effect that DNA molecules go out of the observation area (about 80 μm × 60 μm) by electrophoresis or go out of focus by vertical diffusion. The sampling interval was 0.1 s. From the observed data, about 10 sequences of images (i.e., 10 molecules) at each condition were chosen for further analyses.

3. Results

3.1. Image Data. Figure 2 is an example of the time development of $v_x(t)$, $R_l(t)$, and $R_s(t)$. It is seen that $R_l(t)$ and $v_x(t)$ show large fluctuations from the average value, while fluctuations of $R_s(t)$ remain rather small. As has been reported already,[4-9] the large fluctuations of $R_l(t)$ and $v_x(t)$ are related to the characteristic motion of DNA. Figure 3 shows the actual conformations of DNA at each stage indicated by I–VI in Figure 2:

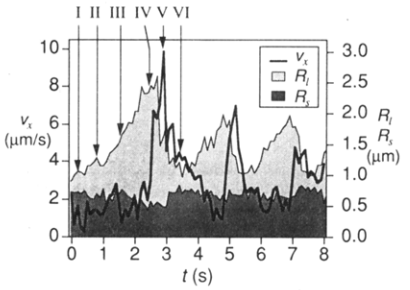

Figure 2. Example of the time development of v_x, R_l, and R_s of T4 DNA during gel electrophoresis. The field strength is 8 V/cm, and the gel concentration is 1.5 wt %.

Figure 3. Digitized images of T4 DNA at the stages I–VI in Figure 2. The scale bar is 20 μm long.

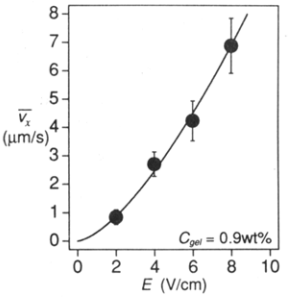

Figure 4. Ensemble averages of v_x of T4 DNA under various field strengths E. The gel concentration is 0.9 wt %. Error bars are the standard deviation calculated for the set of molecules at each condition. A function $\overline{v_x} \propto E^{1.5}$ is shown by the solid curve.

Stage I. A DNA molecule in the gel has a coiled conformation. At this stage, R_l and R_s are about the same size as those in buffer solutions.[17,18]

Stage II. The DNA begins to be stretched since its middle part is caught by a gel fiber.

Stage III. The Λ-conformation of the DNA grows with its apex fixed at the gel fiber. At this stage, the migration velocity $v_x(t)$ becomes the smallest.

Stage IV. The longer arm in the Λ-conformation becomes dominant and begins to pull the other arm. Consequently, the dominant arm becomes longer and the shorter one becomes even shorter.

Stages V and VI. The DNA is released from the gel fiber and shrinks rapidly, retrieving the coiled conformation. During this process, the velocity of migration becomes a maximum.

Before going to the detailed discussion on such time-dependent conformational change, we first describe the results of the time-averaged quantities.

3.2. Average Velocity and Average Size. Figures 4 and 5 show the average velocity $\overline{v_x}$ as a function of the field strength E and the gel concentration C_{gel}. The velocity $\overline{v_x}$ increases in proportion to E^α with $\alpha \sim 1.5$ and decreases in proportion to $C_{gel}{}^\beta$ with $\beta \sim -0.9$. These results are consistent with the standard macroscale gel electrophoresis.[19-23] The values of $\overline{v_x}$ are also in reasonable agreement with reported values obtained by the usual gel electrophoresis; for example, Shikata and Kotaka[23] reported that $\overline{v_x}$ is about 0.6 μm/s under E = 2.5 V/cm and

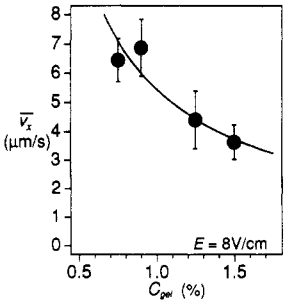

Figure 5. Ensemble averages of v_x of T4 DNA under various gel concentrations C_{gel}. The field strength is 8 V/cm. A function $\overline{v_x} \propto C_{gel}^{-0.9}$ is shown by the solid curve.

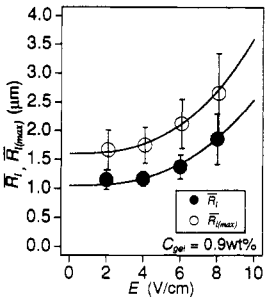

Figure 6. Ensemble averages of R_l of T4 DNA under various field strengths E. The gel concentration is 0.9 wt %. $\overline{R_l}$ are the time averages, and $\overline{R_{l(max)}}$ are the average peak values of R_l. The set of solid curves are to guide the eye.

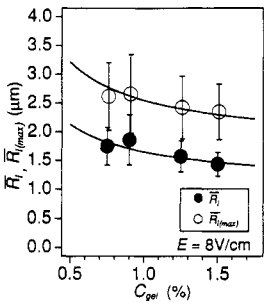

Figure 7. Ensemble averages of R_l of T4 DNA under various C_{gel}. The field strength is 8 V/cm. The set of solid curves are to guide the eye.

C_{gel} = 1.0 wt % agarose. Therefore, we believe that our experimental condition is very similar to that of the usual macroscale gel electrophoresis.

Figures 6 and 7 respectively show how the average size of DNA depends on E and C_{gel}. Here $\overline{R_l}$ denotes the time average of $R_l(t)$ and $\overline{R_{l(max)}}$ denotes the average of the height of the peaks of $R_l(t)$ as in stage V in Figure 2. For given data of the time sequence of $R_l(t)$, the peaks are identified as follows: First, the times at which $R_l(t)$ becomes the local maximum are picked up and numbered as t_1, t_2, ... Then, if the value $R_l(t_i)$ is larger than the threshold value of $\overline{R_l}$ plus the standard deviation of $R_l(t)$ and if it is the largest one in the time interval between $t_i - 0.5$ and $t_i + 0.5$ s, the local peak at t_i is recognized as a true peak. $\overline{R_{l(max)}}$ is the average of about 30 such peaks.

Notice that the average $\overline{R_l}$ increass sharply with the increase of E, while it is rather insensitive to C_{gel}, or decreases slightly as the gel concentration increases.

3.3. Periodic Behavior. Figure 2 suggests that there is a certain kind of periodicity in the motion of DNA. To show this quantitatively, we calculated the autocorrelation

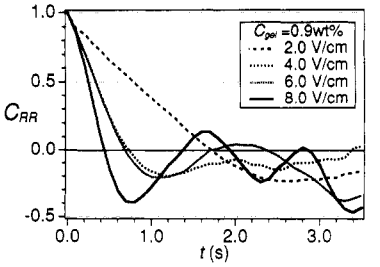

Figure 8. Ensemble averages of autocorrelation functions of R_l under various E. C_{gel} is 0.9 wt %.

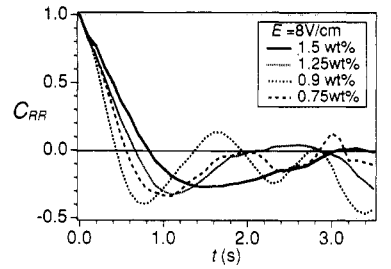

Figure 9. Similar to Figure 8 under various C_{gel}. E is 8 V/cm.

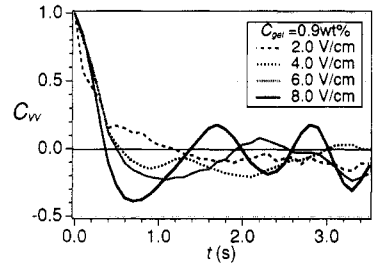

Figure 10. Ensemble averages of autocorrelation functions of v_x under various E. C_{gel} is 0.9 wt %.

function $C_{RR}(t)$ defined by

$$C_{RR}(t) \equiv \frac{\int (R_l(t'+t) - \overline{R_l})(R_l(t') - \overline{R_l})\, dt'}{\int (R_l(t') - \overline{R_l})^2\, dt'} \approx \frac{\sum_i (R_l(t_i+t) - \overline{R_l})(R_l(t_i) - \overline{R_l})}{\sum_i (R_l(t_i) - \overline{R_l})^2} \quad (10)$$

and $C_{vv}(t)$, the autocorrelation function of $v_x(t)$. The results are shown in Figures 8–10.

It is seen that $C_{RR}(t)$ and $C_{vv}(t)$ do not decay monotonically but decay with some oscillation. The oscillatory behavior is not clear in a weak electric field but becomes clearer as the field strength increases. The oscillatory behavior is also seen in the autocorrelation functions of $v_x(t)$, although it is less obvious due to the large noises in $v_x(t)$. Nevertheless, one can see that both $C_{RR}(t)$ and $C_{vv}(t)$ oscillate with a similar characteristic time.

To obtain the characteristic time of oscillation, we took t_0 at which the autocorrelation function $C_{RR}(t)$ first becomes zero and defined the oscillation period τ by

$$\tau \equiv 4t_0 \quad (11)$$

In Figures 11 and 12, τ is plotted against E and C_{gel}, respectively. The period τ decreases as the field strength increases or the gel concentration decreases. This behavior is similar to that of $1/\overline{v_x}$. We shall come back to this point later.

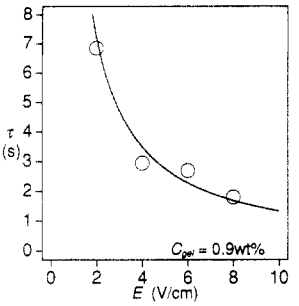

Figure 11. Oscillation period τ estimated from C_{RR} plotted against the field strengths E. C_{gel} is 0.9 wt %. The solid curve is a function $\tau \propto E^{-1.1}$.

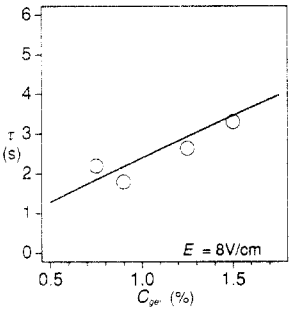

Figure 12. τ plotted against the gel concentrations C_{gel}. E is 8 V/cm. The solid curve is a function $\tau \propto C_{gel}^{0.9}$.

3.4. Phase Difference between $R_l(t)$ and $v_x(t)$. Figure 2 indicates that there is a strong correlation between $R_l(t)$ and $v_x(t)$: the peaks of $R_l(t)$ and $v_x(t)$ take place at about the same time. To study this in more detail, we calculated the cross-correlation function $C_{vR}(t)$ defined by

$$C_{vR}(t) \equiv \frac{1}{T}\int_0^T (v_x(t'+t) - \overline{v_x})(R_l(t') - \overline{R_l})\, dt' \qquad (12)$$

The result (not shown here) indicates that the peak of $v_x(t)$ takes place slightly later than that of $R_l(t)$, and the delay time (about 0.3 s) is rather insensitive to the electric field E and the gel concentration C_{gel}.

3.5. Wave Shapes. Figures 2 and 3 indicate that there is a characteristic pattern in the time development of $R_l(t)$ near the peak: $R_l(t)$ increases slowly but decreases rapidly. To study the shape of $R_l(t)$ near the peak, we calculated the ensemble-averaged shape around the peak in the following way. For a given condition of E and C_{gel}, we chose about 15 peaks in the graphs of $R_l(t)$. We then determined their peak position t_{max} and took the average of $R_l(t)$ for the same value of $t - t_{max}$. The result is shown in Figure 13, where the time is normalized by the characteristic time τ determined by eq 11 and $\overline{R_l}(t - t_{max})$ is normalized by the average peak $\overline{R_l}(0)$. It is seen that the results for different E and C_{gel} can be superimposed in this scaled plot. The slope of $R_l(t)$ after the peak is about 3 times larger than that before the peak, and the ratio is constant and independent of E and C_{gel}.

3.6. Motion of the Front End and the Rear End. To study the motion of DNA near the peak position, we focused our attention on the positions of the center of mass $r_x(t)$, the front end $r_{fx}(t)$, and the rear end $r_{rx}(t)$. The latter two are calculated as follows. If polymer segments are uniformly distributed within an ellipse

$$\frac{(x - x_0)^2}{a^2} + \frac{(y - y_0)^2}{b^2} = 1 \qquad (a > b) \qquad (13)$$

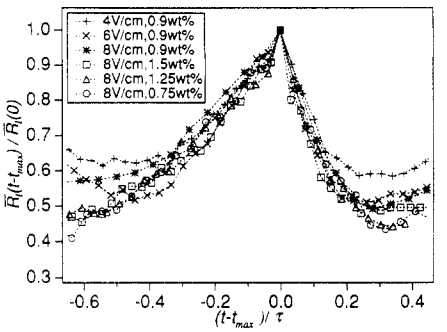

Figure 13. Ensemble averages of time development of R_l of T4 DNA under the various field strengths and gel concentrations. $\overline{R_l}(t - t_{max})$ and $t - t_{max}$ are normalized with respect to $\overline{R_l}(0)$ and τ, respectively.

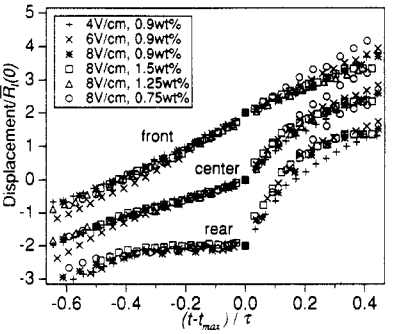

Figure 14. Ensemble averages of the migration distances of the front end, the rear end, and the center of mass of the DNA against time under various conditions in a scaled plot.

R_l is equal to $a/2$. Thus the positions of the front end and the rear end can be estimated by

$$r_{fx}(t) \equiv r_x(t) + 2R_l(t) \qquad (14)$$

$$r_{rx}(t) \equiv r_x(t) - 2R_l(t) \qquad (15)$$

We calculated the average time evolution of these quantities around the peak by the same procedure discussed in section 3.5; for given a electric field and gel concentration, about 15 peaks in the graphs of $R_l(t)$ were chosen, and the averaged displacements $r_x(t)$, $r_{fx}(t)$, and $r_{rx}(t)$ were calculated for the same value of $t - t_{max}$ with $r_x(t_{max})$ taken to be zero. The results are shown in Figure 14 in the scaled plot. It is seen that the time evolution of $r_x(t)$, $r_{fx}(t)$, and $r_{rx}(t)$ can be superimposed in the scaled plot. The interesting point is that the front end moves with almost constant speed, while the rear end shows a stick–slip motion: the rear end stays at a constant position for a while (i.e., for $-0.4 < (t - t_{max})/\tau < 0$) and then starts to move fast trying to catch up the front end. Such motion is understandable if one notes that the rear end corresponds to the apex of the Λ-conformation before the peak of $R_l(t)$ and corresponds to the trailing end of the chain after the peak.

From these data, it becomes thus clear that the front end is moving with almost constant speed and that the fluctuation of the velocity of the center of mass reflects the motion of the rear end.

4. Discussion

4.1. Periodic Behavior of DNA Molecules. We have shown that the autocorrelation functions $C_{RR}(t)$ and $C_{vv}(t)$ do not decay monotonically but decay with some oscillation. Such periodic behavior is surprising, considering that the structure of the gel is random and that the applied

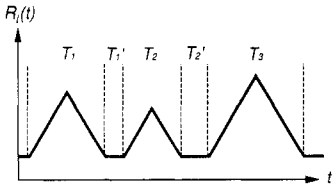

Figure 15. Schematic example of the time evolution of $R_l(t)$ modeled by a series of Λ-shape peaks.

field E is constant. However, the periodic behavior is not an artifact. The characteristic time τ changes consistently with E and C_{gel} as has been shown in the preceding section. Furthermore, it is noted that the periodic behavior has also been observed in a computer simulation. Matsumoto and Doi[14] solved the Langevin equation for a DNA in randomly placed obstacles under strong electric field and showed that the autocorrelation function $C_{RR}(t)$ shows a characteristic oscillation. The characteristic time τ of the oscillation decreased with an increase of the electric field in accordance with our experimental results.

The field dependence of τ indicates that the oscillation is a nonlinear phenomenon driven by the electric field. However, this does not mean that there is a certain kind of regular nonlinear oscillation. Such motion is hardly probable for a DNA moving in a random network. At present, we interpret the origin of the oscillation as follows.

Notice that the conformational change of DNA around the peak of $R_l(t)$ is essentially deterministic; the process going from stage I to V in Figure 3 can be described by a deterministic model such as proposed by Deutsch et al.[10] If the initial configuration at stage I is given, the time evolution of $R_l(t)$ is calculable.[24] On the other hand, the process of going from stage V to VI is not deterministic; when (or which part of) the DNA is caught by the next obstacle depends on the gel structure and is unpredictable. Therefore, the initial configuration for stage I is random. Therefore, time development of $R_l(t)$ involves a stochastic factor. However, if the characteristic time of the process from stage V to VI is much shorter than the characteristic time needed for stages I to V, the autocorrelation function can have an oscillation. We can demonstrate this by a simple example.

Let us suppose that, during stages I to VI, $R_l(t)$ increases or decreases linearly with time. Thus the time evolution of $R_l(t)$ may be modeled by a series of Λ-shape peaks, where each Λ peak represents one cycle of elongation and contraction of DNA (see Figure 15). The width T of the Λ peak and the separation T' between the Λ peaks are not necessarily constant. As long as the fluctuations of T and T' are small, however, the autocorrelation function of $R_l(t)$ can show a damped oscillation. For an illustrative purpose, we calculated the autocorrelation function $C_{RR}(t)$ assuming that the distribution $P(T)$ is Gaussian and $P(T')$ is Poissonian:

$$P(T) = (2\pi\Delta^2)^{-1/2} \exp\left[-\frac{(T-\overline{T})^2}{2\Delta^2}\right] \quad (16)$$

$$P(T') = \lambda \exp[-\lambda T'] \quad (17)$$

Here, $\overline{T}$ is the mean width of a peak, Δ^2 is its variance, and $1/\lambda$ is the mean separation time between the Λ peaks. The calculation is described in the appendix, and the result is shown in Figure 16. Notice that the correlation function becomes oscillatory even if $\Delta/\overline{T}$ is as large as 0.5.

Although the "periodicity" in the graph of $R_l(t)$ is only approximate, the notion is useful in interpreting various data. In Figure 17, we plotted $\overline{R}_{l(max)}/\overline{v}_x$ against the

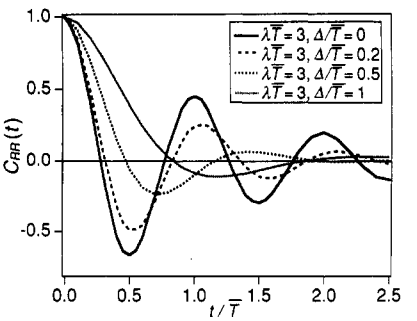

Figure 16. Examples of the autocorrelation function of $R_l(t)$ modeled by a series of Λ-shape peaks.

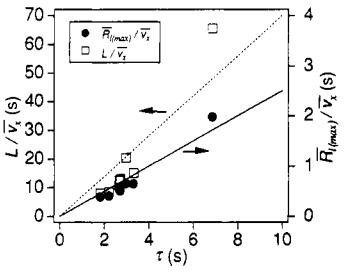

Figure 17. Plots of $\overline{R}_{l(max)}/\overline{v}_x$ vs τ and $L/\overline{v}_x$ vs τ under various E and C_{gel}. The solid line is the function of $\overline{R}_{l(max)}/\overline{v}_x = \tau/4$. The dotted line is to guide the eye.

period of the cycle τ. Although the scatter of the data is significant, one can see that the points are roughly on the line $\overline{R}_{l(max)}/\overline{v}_x = \tau/4$. Notice that, if the separation time T' is negligible, i.e., if the DNA is immediately caught by a new obstacle when it slides off the previous obstacle, the average step length of the cyclic motion is $2a = 4\overline{R}_{l(max)}$, where a is the radius of the longer axis of the ellipse defined in eq 13. Figure 17 thus indicates that the DNA motion can be modeled by an inch-worm-like motion; the average step length is $4\overline{R}_{l(max)}$ and the period is τ. In Figure 17, we also showed the plot of $L/\overline{v}_x$ against τ since it has been conjectured[25] that the characteristic time of the fluctuation is on the order of $L/\overline{v}_x$. (L is the contour length of the DNA.) In this plot, however, the scatter of the data points is larger than that for the plot of $\overline{R}_{l(max)}/\overline{v}_x$ vs τ.

4.2. Relation to "Antiresonance" Phenomena. In recent works, detailed descriptions of dynamics of a DNA molecule during gel electrophoresis were given by computer simulations.[13,26,27] In these reports, it has been conjectured that the time needed to go through one cycle, which corresponds to our characteristic time τ, is closely related to the phenomenon of mobility minimum (or antiresonance[15]) in nonsteady electric field.[23,25,28,29] We now examine whether such a relation exists for real systems.

In the field inversion gel electrophoresis (FIGE), the electric field is varied as

$$E(t) = \begin{cases} E_0 & 0 < t < t_1 \\ -E_0 & t_1 < t < t_1 + t_2 \end{cases} \quad (18)$$

with a period $t_1 + t_2$. Kobayashi et al.[25] reported that the mobility becomes minimum at a certain period T_{min}, which is about 8 s in the case of T4 DNA when $E = 7.72$ V/cm, $t_1/t_2 = 3$, and $C_{gel} = 1$ wt %. They also reported that T_{min} decreases with increases of E. Heller et al.[28] reported that this period depends on the E as

$$T_{min} \propto E^{-1.3} \quad (19)$$

This field dependence is roughly consistent with that found in Figure 11.

Shikata and Kotaka[23] carried out a gel electrophoresis with a biased sinusoidal field $E(t) = E_b + E_s \sin(2\pi ft)$ and reported that the mobility of T4 DNA takes a local minimum at a certain frequency f_p which they call the pin-down frequency. In the case of T4 DNA, $1/f_p$ is about 8 s when E_b = 2.5 V/cm, E_s = 7.5V/cm and about 2.5 s when E_b = 7.5 V/cm, E_s = 12.5V/cm (C_{gel} is equal to 1.0 wt %) in both cases. The period $1/f_p$ has a field dependence similar to that we obtained here. They also reported that $1/f_p$ depends on C_{gel} as

$$1/f_p \propto C_{gel} \tag{20}$$

This dependence of the gel concentration is very similar to our result shown in Figure 12. Therefore, the close relation between the periodic behavior in the steady field gel electrophoresis and the antiresonance phenomena in the nonsteady field gel electrophoresis is also confirmed for real systems.

We have shown that, in one cycle of the DNA motion, the elongation takes place slowly, but the contraction is rapid (see Figure 13). The ratio of the speed $|dR_l/dt|_{elongation}/|dR_l/dt|_{contraction}$ is about 1/3 and independent of E and C_{gel}. It is interesting that this ratio approximately corresponds to the optimum ratio t_2/t_1 of the pulse duration time of the field inversion gel electrophoresis. We conjecture that this has the following reason. Suppose that the field is reversed at stage IV, after which the DNA will strink to conformation I. If the conditions $t_1|dR_l/dt|_{elongation} = t_2|dR_l/dt|_{contraction}$ and $t_1 + t_2 = \tau$ (τ = oscillation period, see eq 11) are satisfied, the conformation of DNA changes from I to IV cyclically, and its center of mass will not migrate. This will cause a large minimum in the mobility. On the other hand, if the ratio between the forward and the backward switch times is greater than 3, the switch time does not match the stretching and recoil processes of DNA molecules even if the condition $t_1 + t_2 = \tau$ is satisfied. This will weaken the antiresonance. Macroscale FIGE experiments may encourage our supposition; in FIGE experiments, a ratio of 3 between forward and backward switch times brings good resolution and has been generally taken in various conditions. In addition, it is known that using a ratio greater than 3 decreases resolution.[29] The above interpretation is qualitative. To confirm this, direct observation of DNA in FIGE and a quantitative modeling of DNA dynamics in the gel electrophoresis are needed. We applied a similar experimental technique to study the motion of DNA molecules during nonsteady field gel electrophoresis, the results of which are reported elsewhere.

Acknowledgment. The authors thank K. Ono for his technical assistance. This study has been financially supported by a Grant-in-Aid for a Creative Basic Research (Human Genome Program), No. 05NP0501, from the Ministry of Education, Science, and Culture, Japan.

Appendix: Calculation of the Autocorrelation Function of a Model Process

Here we calculate the autocorrelation function for a model process described in Figure 15. We assume that each Λ-shape peak in Figure 15 is represented by the following function:

$$f(t;T) = \begin{cases} 0 & t < 0 \\ t & 0 < t < T/2 \\ T - t & T/2 < t < T \\ 0 & T < t \end{cases} \tag{A1}$$

Notice that the slope df/dt is independent of T. Thus $R_l(t)$ is written as

$$R_l(t) = \sum_{n=-\infty}^{\infty} f(t-t_n;T_n) + \text{const.} \tag{A2}$$

with

$$t_n = \sum_{m=0}^{n-1} (T_m + T'_m) \tag{A3}$$

where T_n and T'_n are random variables whose probabilities are given by eqs 16 and 17, respectively.

To calculate the autocorrelation function, we use the Fourier transform:

$$\begin{aligned} R_l(\omega) &= \int_{-\infty}^{\infty} dt\, e^{i\omega t} R_l(t) \\ &= \sum_{n=-\infty}^{\infty} e^{i\omega t_n} f(\omega;T_n) \end{aligned} \tag{A4}$$

where

$$\begin{aligned} f(\omega;T) &= \int_{-\infty}^{\infty} dt\, e^{i\omega t} f(t;T) \\ &= \frac{1}{\omega^2}(2e^{i\omega T/2} - e^{i\omega T} - 1) \end{aligned} \tag{A5}$$

Then

$$\begin{aligned} \langle |R_l(\omega)|^2 \rangle &= \sum_{n,m} \langle e^{i\omega(t_n - t_m)} f(\omega;T_n)\, f^*(\omega;T_m) \rangle \\ &\equiv \sum_{n,m} I(n,m) \end{aligned} \tag{A6}$$

Each term on the right-hand side of eq A6 depends on $n - m$ only as $I_{n-m} \equiv I(n,m)$ and can be calculated using the fact that T_n and T'_n are independent of each other. For example, we have for $n > 0$

$$\begin{aligned} I_n &= \langle \exp[i\omega \sum_{m=0}^{n-1} (T_m + T'_m)] f(\omega;T_n)\, f^*(\omega;T_0) \rangle \\ &= \langle e^{i\omega T'} \rangle^n \langle e^{i\omega T} \rangle^{n-1} \langle e^{i\omega T} f^*(\omega;T) \rangle \langle f(\omega;T) \rangle \end{aligned} \tag{A7}$$

Substituting this into eq A6, we have

$$\langle |R_l(\omega)|^2 \rangle = \langle |f(\omega;T)|^2 \rangle + 2\mathrm{Re}\left[\frac{\langle e^{i\omega T'} \rangle \langle e^{i\omega T} f^*(\omega;T) \rangle \langle f(\omega;T) \rangle}{1 - \langle e^{i\omega T} \rangle \langle e^{i\omega T'} \rangle} \right] \tag{A8}$$

The averages in eq A8 can be easily calculated using eqs 16 and 17. Substituting these results and doing the numerical integration for

$$C_{RR}(t) = \int_{-\infty}^{\infty} \frac{d\omega}{2\pi} e^{-i\omega t} \langle |R_l(\omega)|^2 \rangle \tag{A9}$$

we obtain Figure 16.

References and Notes

(1) Nordén, B.; Elvingson, C.; Jonsson, M.; Åkerman, B. *Quart. Rev. Biophys.* **1991**, *24*, 103 and references therein.

(2) Zimm, B. H.; Levene, S. D. *Quart. Rev. Biophys.* **1992**, *25*, 171 and references therein.
(3) Matsumoto, S.; Morikawa, K.; Yanagida, M. *J. Mol. Biol.* **1981**, *152*, 501.
(4) Smith, S. B.; Aldridge, P. K.; Callis, J. B. *Science* **1989**, *243*, 203.
(5) Schwartz, D. C.; Koval, M. *Nature* **1989**, *338*, 520.
(6) Gurrieri, S.; Rizzarelli, E.; Beach, D.; Bustamante, C. *Biochemistry* **1990**, *29*, 3396.
(7) Rampino, N. J. *Biopolymers* **1991**, *31*, 1009.
(8) Howard, T. D.; Holzwarth, G. *Biophys. J.* **1992**, *63*, 1487.
(9) Masubuchi, Y.; Oana, H.; Ono, K.; Matsumoto, M.; Doi, M.; Minagawa, K.; Matsuzawa, Y.; Yoshikawa, K. *Macromolecules* **1993**, *26*, 5269.
(10) Deutsch, J. M.; Madden, T. L. *J. Chem. Phys.* **1989**, *90*, 2476.
(11) Shaffer, E. O., II; Olvera de la Cruz, M. *Macromolecules* **1989**, *22*, 1351.
(12) Duke, T. A. J. *J. Chem. Phys.* **1990**, *93*, 9049.
(13) Zimm, B. H. *J. Chem. Phys.* **1991**, *94*, 2187.
(14) Matsumoto, M.; Doi, M. *Mol. Simul.*, in press.
(15) Carle, G. F.; Frank, M.; Olson, M. V. *Science* **1986**, *232*, 65.
(16) Yoshikawa, K.; Matsuzawa, Y.; Minagawa, K.; Doi, M.; Matsumoto, M. *Biochem. Biophys. Res. Commun.* **1992**, *188*, 1274.
(17) Matsumoto, M.; Sakaguchi, T.; Kimura, M.; Doi, M.; Minagawa, K.; Matsuzawa, Y.; Yoshikawa, K. *J. Polym. Sci., Part B: Polym. Phys.* **1992**, *30*, 779.
(18) Matsuzawa, Y.; et al., unpublished data.
(19) Stellwagen, N. C. *Biopolymers* **1985**, *24*, 2243.
(20) Slater, G. W. *Biopolymers* **1988**, *27*, 509.
(21) Holzwarth, G.; Platt, K. J.; McKee, C. B.; Whitcomb, R. W.; Crater, G. D. *Biopolymers* **1989**, *28*, 1043.
(22) Calladine, C. R.; Collis, C. M.; Drew, H. R.; Mott, M. R. *J. Mol. Biol.* **1991**, *221*, 981.
(23) Shikata, T.; Kotaka, T. *Macromolecules* **1991**, *24*, 4868.
(24) Akiyama, T.; et al., unpublished work.
(25) Kobayashi, T.; Doi, M.; Makino, Y.; Ogawa, M. *Macromolecules* **1990**, *23*, 4480.
(26) Deutsch, J. M. *J. Chem. Phys.* **1989**, *90*, 7436.
(27) Duke, T. A. J.; Viovy, J. L. *J. Chem. Phys.* **1992**, *96*, 8552.
(28) Heller, C.; Pohl, F. M. *Nucleic Acids Res.* **1989**, *17*, 5989.
(29) Birren, B.; Lai, E. *Pulsed Field Gel Electrophoresis*; Academic Press, Inc.: San Diego, CA, 1993.